OUKA
The University of Osaka
Institutional Knowledge Archive

Title	Cr^{6+} Loaded Lewis Acidic Sn-Beta Zeolites as Reusable Catalysts for Selective Production of Light Olefins via Polyolefin Cracking
Author(s)	Kokuryo, Shinya; Tsubota, Soshi; Miyake, Koji et al.
Citation	Advanced Sustainable Systems. 2024, 9(3), p. 2400625
Version Type	VoR
URL	https://hdl.handle.net/11094/98883
rights	This article is licensed under a Creative Commons Attribution 4.0 International License.
Note	

The University of Osaka Institutional Knowledge Archive : OUKA

https://ir.library.osaka-u.ac.jp/

The University of Osaka

Check for updates

ADVANCED SUSTAINABLE SYSTEMS
www.advsustainsys.com

Cr^{6+} Loaded Lewis Acidic Sn-Beta Zeolites as Reusable Catalysts for Selective Production of Light Olefins via Polyolefin Cracking

Shinya Kokuryo, Soshi Tsubota, Koji Miyake,* Yoshiaki Uchida, Atsushi Mizusawa, Tadashi Kubo, and Norikazu Nishiyama*

Catalysts for the selective recovery of light olefins from polyolefins should be developed to save limited fossil resources. It is previously revealed that Brønsted acid-free Sn-Beta zeolites selectively produced light olefins from polyolefin cracking. Brønsted acid sites ionize olefins by protonation and the generated carbenium ions are converted into other hydrocarbons via various reactions, thereby the elimination of their effects led to the improvement of light olefin production ability. However, the deactivation of zeolites by coke deposition is a critical problem for industrialization. Inhibition of coking deactivation is previously achieved by doping Cr^{6+} species connected to silanol groups in zeolites. This work aimed to inhibit coke deposition and realize selective and continuous production of light olefins through repetitive polyolefin catalytic cracking. Sn-Beta zeolites are prepared with various crystallinity by changing the feed fluoride ions content in their synthesis and found that their activity on low-density polyethylene (LDPE) cracking strongly depended on the feed F/Si ratios, implying the active sites for polyolefin cracking are Lewis acidic open-Sn sites. Moreover, Cr^{6+}-doped Sn-Beta zeolites showed over 45% light olefin yields even in the third LDPE cracking test, although excess Cr adding led to reduce the catalytic activity of Sn-Beta zeolites.

1. Introduction

Catalytic cracking of polyolefins has been an important topic for the development of sustainable recycling systems of plastic materials, and so far, numerous efforts have been devoted to the optimization of the catalysts.[1–6] Zeolites are effective catalysts for polyolefin cracking because of their excellent physicochemical properties and high hydrothermal stability.[7–10] Their acidity catalyzes the cracking reactions,[7,11] and their uniform pore structure enables the control of product distributions to some extent.[10,12–14] Moreover, specific functions are afforded to zeolites depending on their design, and they have been applied to various reactions.[15–21]

Selective recovery systems of high-value products, especially light olefins, from polyolefins should be developed.[22] Light olefins are important as key feedstocks and platform molecules in the petrochemical and chemical industries, used for producing polymers, synthetic fibers, rubbers, and plastics.[23–25] Although product distributions can be controlled physically to some extent depending on zeolitic pore structure,[10,12–14] chemical approaches based on the reaction mechanism of polyolefin cracking are needed for further selectivity.

While thermal cracking (noncatalytic) of polyolefin proceeds via a radical mechanism, catalytic cracking with zeolites is catalyzed by their acid sites via the carbenium ion mechanism.[7] These carbenium ions are generated by both Brønsted and Lewis acid sites in zeolites by protonation and abstraction of a hydride ion, respectively.[7,11,26–29]

We previously revealed that Brønsted acid-free Sn-Beta zeolites selectively produced light olefins from polyolefin cracking.[30] Brønsted acid sites ionize olefins by protonation and the generated carbenium ions are converted into other hydrocarbons via various reactions (isomerization, oligomerization, cyclization, aromatization, etc.).[31–33] Therefore, eliminating Brønsted acidity can protect generated light olefins from conversion into other hydrocarbons, leading to an increase in their yields. As mentioned above, Lewis acid sites also generate carbenium ions by the abstraction of hydride ions from polymer molecules. We have

S. Kokuryo, S. Tsubota, K. Miyake, Y. Uchida, N. Nishiyama
Division of Chemical Engineering
Graduate School of Engineering Science
Osaka University
1-3 Machikaneyama, Toyonaka, Osaka 560-8531, Japan
E-mail: skokuryo@cheng.es.osaka-u.ac.jp;
kojimiyake@cheng.es.osaka-u.ac.jp

K. Miyake, N. Nishiyama
Innovative Catalysis Science Division
Institute for Open and Transdisciplinary Research Initiatives (ICS-OTRI)
Osaka University
Suita, Osaka 565-0871, Japan

A. Mizusawa, T. Kubo
AC Biode Co.
Ltd. 498-6 Iwakura Hanazono, Sakyo, Kyoto 606-0024, Japan

The ORCID identification number(s) for the author(s) of this article can be found under https://doi.org/10.1002/adsu.202400625

© 2024 The Author(s). Advanced Sustainable Systems published by Wiley-VCH GmbH. This is an open access article under the terms of the Creative Commons Attribution License, which permits use, distribution and reproduction in any medium, provided the original work is properly cited.

DOI: 10.1002/adsu.202400625

prepared Lewis acidity-improved zeolites (defect-rich zeolites[34] and Lewis acidic metals added zeolites[35–37]) and found that enhancing the Lewis acidity of zeolites promotes polyolefin cracking. Similarly, Lewis-acidic Sn-Beta zeolites without Brønsted acidity promote polyolefin cracking via the carbenium ion mechanism at lower temperatures than thermal cracking (radical mechanisms) occurs, and they enable the increase in the light olefin yields. However, the active Sn species for polyolefin cracking was not specified in detail in our previous study,[30] therefore one aim of this study is their elucidation by controlling the zeolitic crystallinity using fluoride ions.

Moreover, coke deposition inevitably deactivates the catalysts and cannot be used repeatedly without oxidative regeneration accompanied by the generation of toxic gases depending on the type of plastic molecules.[38–41] In the case of polyolefins, regeneration of catalysts leads to CO_2 emission. The polycyclization of aromatics forms these coke materials[42] and they cause pore blocking and covering active sites, resulting in deactivation.[43] We previously achieved inhibition of coking deactivation by doping Cr^{6+} species connected to silanol groups in zeolites.[44,45] Silanol groups in zeolites stabilize the Cr^{6+} species and catalyze the dehydrogenation of alkanes.[46,47] Various alkanes are produced during polyolefin cracking, thereby hydrogen can be generated by Cr^{6+}. Then, aromatics are decomposed by zeolitic acid sites via hydrogenation and carbenium ion mechanism[48] with hydrogen generated by Cr^{6+}, resulting in coking inhibition. We have found that these Cr^{6+}-doped zeolites can be used repeatedly without regeneration for low-density polyethylene (LDPE) cracking while maintaining their activity.[44,45] Therefore, integrating these above insights can realize the development of appropriate zeolite catalysts for polyolefin cracking.

This work aimed to understand the active Sn sites in Brønsted acid-free Sn-Beta zeolites for polyolefin cracking and dope Cr^{6+} while maintaining their activity; realizing the selective and continuous production of light olefins through repetitive polyolefin catalytic cracking without oxidative regeneration.

2. Results and Discussion

2.1. Sn-Beta Zeolites

Sn-Beta zeolites with high Sn content were synthesized through interzeolite transformation from MWW-type zeolites. The detailed synthesis method is described in the experimental section. First, B-MWW was synthesized and deboronated by acid treatment as shown in Figure S1 (Supporting Information). After acid treatment, the retainment of the MWW structure was confirmed from XRD patterns, N_2 adsorption isotherms, and TEM images. FT-IR spectra of adsorbed pyridine on B-MWW and deB-MWW were recorded and peaks of pyridine adsorbed on Brønsted acid sites derived from framework boron species were not detected for de-BMM, indicating almost all boron species were eliminated by the acid treatment.

After Sn introduction to the deB-MWW, Sn-Beta zeolites were synthesized via interzeolite transformation of the Sn-MWW with different feed F/Si molar ratios. All Sn-Beta-*x*F samples showed XRD patterns derived from Beta-type zeolites[49,50] and the peaks of the (302) plane shifted by changing feed F/Si ratios as shown in **Figure** 1a,b, indicating that the interzeolite transformation of MWW to Beta was completed and the (302) d-spacing was expanded depending on the incorporated Sn amount because atomic radii of Sn is larger than that of Si. Meanwhile, all samples showed no peaks derived from bulk SnO_2, suggesting highly dispersed Sn species in Sn-Beta zeolites. The physical properties of Sn-Beta-*x*F were evaluated by N_2 adsorption measurements as shown in Figure 1c and listed in **Table 1**. The external surface area (S_{ext}) was decreased and the micropore volume (V_{micro}) was increased with an increase in the F/Si ratio because F^- ions enhance the crystallization and reduce the structural defects in zeolite synthesis, leading to high crystallinity.[51–53] From the TEM images, aggregated nanoparticles were observed in all samples including Sn-MWW, indicating that the excess amount of Sn formed SnO_2 on the MWW surface and remained after interzeolite transformation to Beta (Figure 1d).

These SnO_2 nanoparticles were also found in UV–vis spectra (peaks at ≈250 nm), while peaks at ≈205 nm derived from the framework tetra-coordinated Sn species were detected as shown in **Figure** 2a.[54,55] To investigate the state of Sn species in detail, Sn 3d XPS spectra for Sn-Beta-*x*F were recorded as shown in Figure 2b. All samples showed peaks derived from tetra-coordinated framework Sn ($3d_{5/2}$: 487.7 eV, $3d_{3/2}$: 496.2 eV) and extra-framework Sn oxides ($3d_{5/2}$: 494.5 eV, $3d_{3/2}$: 486.0 eV),[55] and the F^- content had almost no effect on their chemical state. Meanwhile, the area ratios of (framework Sn)/(extra framework SnO_2) in Sn-Beta-0.2F were smaller than that of other Sn-Beta samples due to the lack of F^- content in the synthesis gel (Table S1, Supporting Information). In addition, the framework Sn ratios decreased with the increase in feed F^- content. These results indicate that the crystallinity of zeolites strongly affects the state of Sn and the decrease in the amount of the zeolitic structural defects leads to the prevention of the incorporation of Sn to their framework. To investigate the fine chemical state of Si species in zeolites, curve fitting analysis for Si 2p XPS spectra was conducted as shown in Figure 2c. All samples showed peaks derived from tetra-coordinated Si^{4+} and Si—OH at ≈104 eV and 100 eV, respectively. The percentage of Si^{4+} to whole Si in zeolites is calculated using their areas and listed in Table S2 (Supporting Information). The percentage of framework Si^{4+} increased with the increase in the feed F^- amount, indicating the enhancement of crystallinity. Moreover, the peaks derived from framework Si^{4+} shifted to lower binding energy with the increase in F^- amount. The electronegativity of Sn is smaller than that of Si, thereby the binding energy of Si^{4+} should shift to higher by incorporating Sn into the zeolitic framework. Therefore, these results mean that the framework Sn amount was decreased with the increase in F^- amount (enhancement of crystallinity) because of the difference in atomic radii of Si and Sn. Moreover, the acidic properties of Sn-Beta samples were evaluated by FT-IR spectra of adsorbed pyridine (Figure 2d). All samples showed peaks of pyridine adsorbed on Lewis acid sites at ≈1450 cm^{-1},[56] while they have no Brønsted acidity. The Lewis acid amount of Sn-Beta-0.2F was smaller than that of other Sn-Beta samples and its amount was decreased with the increase in F/Si ratios when F/Si is over 0.25. F^- ions reduce defect sites and promote the generation of closed-Sn sites during the synthesis, thereby the increase in F/Si ratios led to decreased Lewis acidity. These results indicate that framework open-Sn sites mainly served as Lewis acid sites.

© 2024 The Author(s). Advanced Sustainable Systems published by Wiley-VCH GmbH

23667486, 0, Downloaded from https://onlinelibrary.wiley.com/doi/10.1002/adsu.202400625 by The University Of Osaka, Wiley Online Library on [20/11/2024]. See the Terms and Conditions (https://onlinelibrary.wiley.com/terms-and-conditions) on Wiley Online Library for rules of use; OA articles are governed by the applicable Creative Commons License

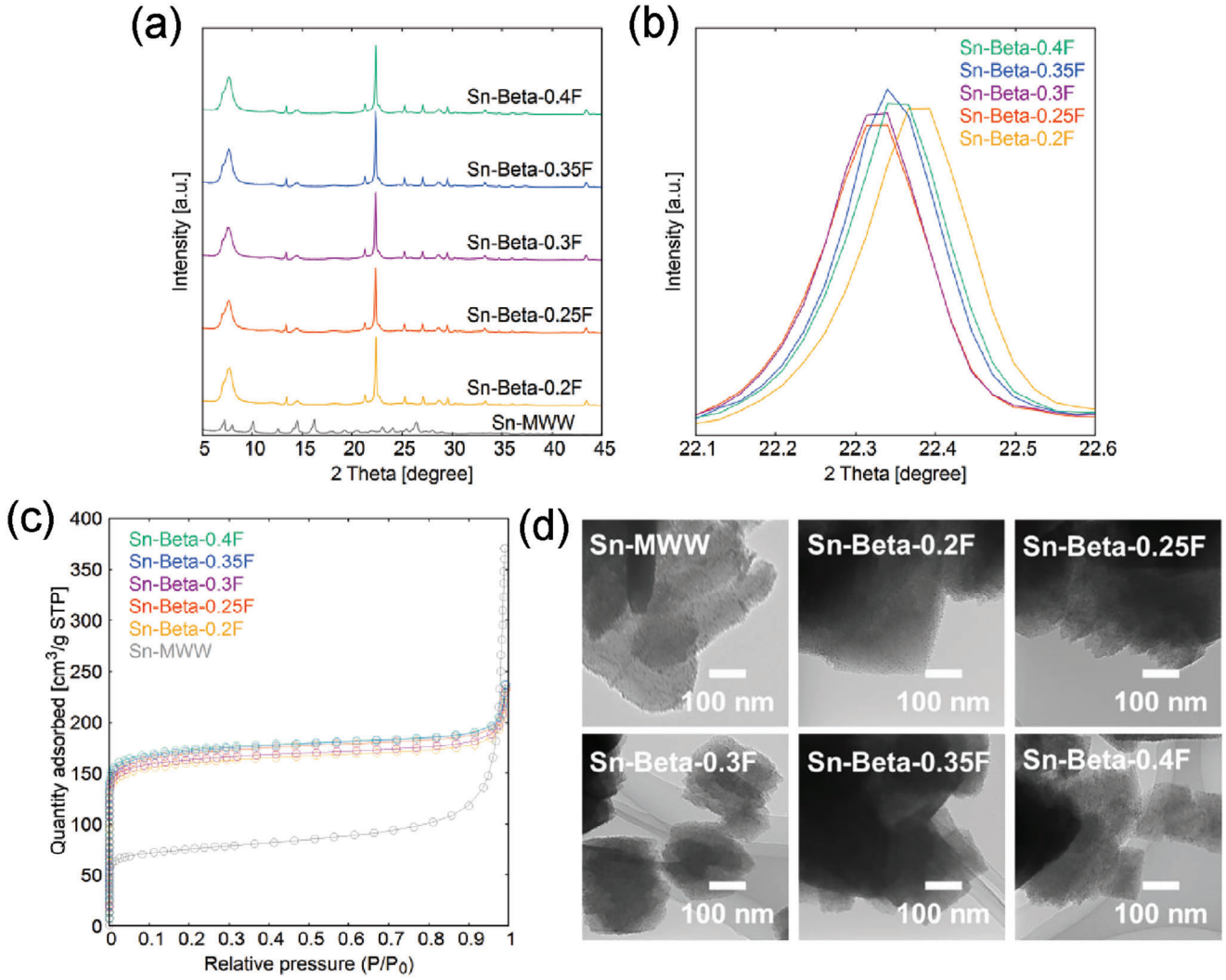

Figure 1. a). XRD patterns of Sn-MWW and Sn-Beta-*x*F. b) The peak at $2\theta \approx 23°$ is magnified to focus on the shift. c) N_2 adsorption isotherms and d) TEM images of Sn-MWW and Sn-Beta-*x*F.

Table 1. Physicochemical properties of Sn-MWW and Sn-Beta-*x*F.

	Si/Sn [-]	S_{BET} [m^2/g]	S_{ext} [m^2/g]	S_{micro} [m^2/g]	V_{micro} [cm^3/g]
Sn-MWW	65.6	365.2	95.4	269.8	0.062
Sn-Beta-0.2F	59.0	836.4	24.4	812.0	0.247
Sn-Beta-0.25F	56.2	860.6	24.3	836.3	0.258
Sn-Beta-0.3F	63.6	814.2	22.9	791.3	0.244
Sn-Beta-0.35F	65.6	876.5	21.7	854.8	0.264
Sn-Beta-0.4F	72.1	895.2	22.0	873.2	0.264

The cracking activities of synthesized Sn-Beta zeolites were evaluated using Thermogravimetric (TG) analysis with LDPE (**Figure** 3a). All samples started to catalyze the reaction at lower temperatures than thermal cracking (radical mechanisms) occurred and Sn-Beta-0.25F with high Lewis acidity recorded the lowest cracking temperature among Sn-Beta zeolites. As shown in Figure 3b, T_{half} value was plotted with the F/Si ratio in the synthetic gel of Sn-Beta zeolites. Here, the T_{half} value was defined as the temperature at which the LDPE conversion rate reached 50%. Sn-Beta-0.2F showed almost no cracking activity due to its lack of Lewis acidity. Moreover, the correlation between the T_{half} value and feed F^- amount was found when F/Si ratios were over 0.25. The cracking temperature depended on the Lewis acidity: the number of open-Sn sites, thereby the ex-

© 2024 The Author(s). Advanced Sustainable Systems published by Wiley-VCH GmbH

23667486, 0, Downloaded from https://onlinelibrary.wiley.com/doi/10.1002/adsu.202400625 by The University Of Osaka, Wiley Online Library on [20/11/2024]. See the Terms and Conditions (https://onlinelibrary.wiley.com/terms-and-conditions) on Wiley Online Library for rules of use; OA articles are governed by the applicable Creative Commons License

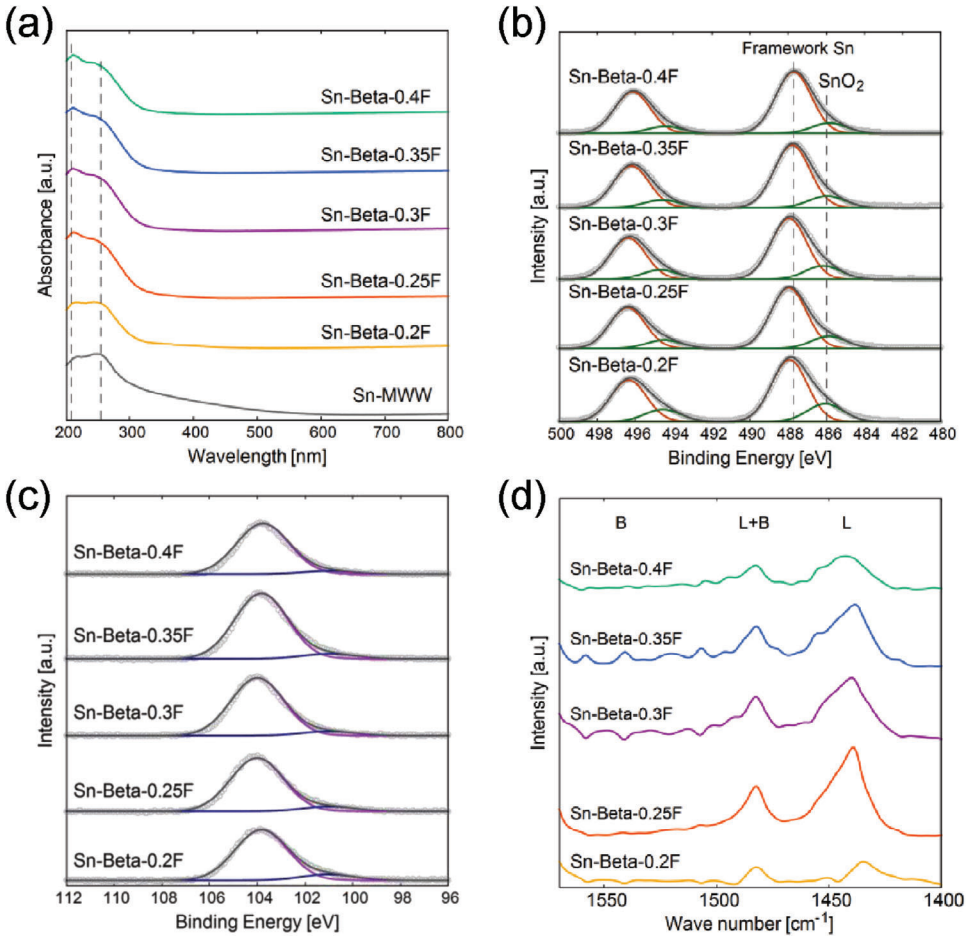

Figure 2. a). UV–vis and b) Sn 3d XPS and c) Si 2p XPS spectra of Sn-MWW and Sn-Beta-*x*F. d) FT-IR spectra of adsorbed pyridine on Sn-Beta-*x*F.

cess F^- addition led to reduced catalytic activity for polyolefin cracking.

The product distributions over LDPE cracking with synthesized Sn-Beta samples were analyzed using gas chromatography (**Figure 4**). All Sn-Beta samples produced gaseous products at almost the same amount as commercial Beta zeolites, while the gas yield without catalysts was less than 50% as shown in Figure 4a. In addition, the selectivity of C6+ was reduced by using zeolite catalysts including Sn-Beta, and especially, Sn-Beta-0.25F and Sn-Beta-0.3F recorded higher selectivity of lighter hydrocarbons, suggesting the product selectivity strongly depends on the number of Lewis acidic open-Sn sites (Figure 4b). These results also indicate that the cracking reaction was catalyzed by the Lewis acid sites in Sn-Beta and proceeded via the carbenium ion mechanism. Moreover, the yields of light olefins increased by more than 20% using Sn-Beta-0.25F and Sn-Beta-0.3F compared to commercial Beta, as shown in Figure 4d: the same tendency as our previous study.[30]

2.2. Cr/Sn-Beta Zeolites

All Cr/Sn-Beta samples showed XRD patterns derived from Beta-type zeolites[48,49] and no peaks derived from impurities, suggesting highly dispersed Cr species in Cr/Sn-Beta zeolites as shown in **Figure 5**a. The elementary compositions of the samples were measured by EDS analysis and listed in **Table 2**. The Si/Cr ratios of Cr/Sn-Beta were decreased with the increase in the feed Cr amount, while the Si/Sn ratios were almost the same in all samples. The physical properties of Cr/Sn-Beta zeolites were evaluated by N_2 adsorption measurements as shown in Figure 5b and listed in Table 2. Although the porosity was slightly decreased with the increase in the loading Cr amount, the physical properties of Cr/Sn-Beta samples were almost the same as that of Cr-free Sn-Beta. In addition, TEM images of all Cr/Sn-Beta zeolites show the same morphology as before the Cr loading although the existence of Cr_2O_3 cannot be completely ruled out, and aggregated Cr_2O_3 was not observed on their surface (Figure 5c). These results indicate that the Cr loading was completed with few aggregations of Cr oxides and blocking of zeolitic micropores.

Next, UV–vis and FT-IR spectra were recorded to investigate the fine chemical state of Cr species in zeolites. All Cr-loaded samples showed peaks at ≈350 and 460 nm derived from Cr^{6+},[57] and a peak at 600 nm (Cr^{3+})[58] was detected only in Cr/Sn-Beta(1.5) as shown in **Figure 6**a, indicating that Cr^{6+} is preferentially formed during the Cr loading (calcination) and an excess amount of Cr formed Cr_2O_3 similar to our previous work.[44] Moreover, all Cr/Sn-Beta samples show peaks at ≈205

© 2024 The Author(s). Advanced Sustainable Systems published by Wiley-VCH GmbH

23667486, 0, Downloaded from https://onlinelibrary.wiley.com/doi/10.1002/adsu.202400625 by The University Of Osaka, Wiley Online Library on [20/11/2024]. See the Terms and Conditions (https://onlinelibrary.wiley.com/terms-and-conditions) on Wiley Online Library for rules of use; OA articles are governed by the applicable Creative Commons License

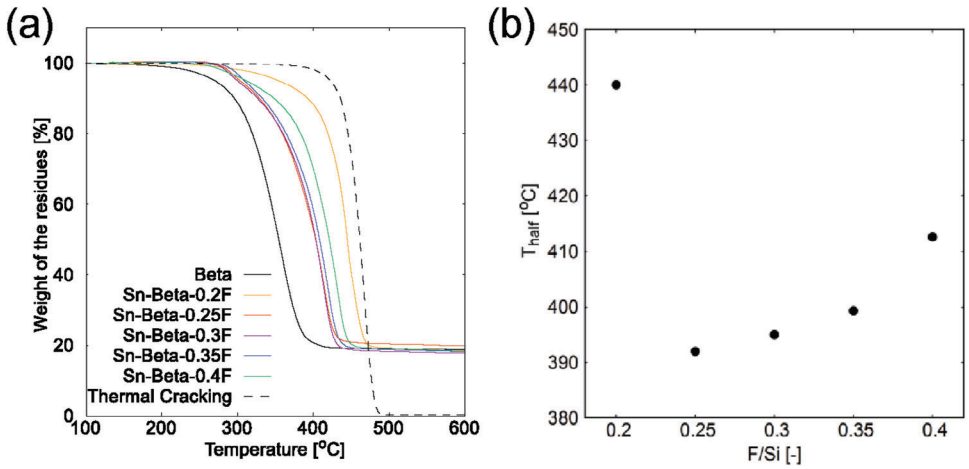

Figure 3. a). TG curves were obtained during catalytic cracking of LDPE with commercial H^+-Beta (TOSOH, SiO_2/Al_2O_3 = 28.9) and Sn-Beta-*x*F. b) Dependence of T_{half} value on the feed F/Si ratio of Sn-Beta zeolites.

Table 2. Physicochemical properties of Sn-Beta-0.25F and Cr/Sn-Beta(*y*).

	Si/Sn [-]	Si/Cr [-]	S_{BET} [m^2/g]	S_{ext} [m^2/g]	S_{micro} [m^2/g]	V_{micro} [cm^3/g]
Sn-Beta-0.25F	56.2	-	860.6	24.3	836.3	0.258
Cr/Sn-Beta(0.5)	58.2	363.7	872.2	26.9	871.9	0.256
Cr/Sn-Beta(0.75)	57.5	139.4	716.0	23.1	715.8	0.210
Cr/Sn-Beta(1)	53.3	106.7	701.4	25.1	701.2	0.202
Cr/Sn-Beta(1.5)	58.3	68.0	707.2	24.0	706.7	0.205

nm derived from the framework tetrahedrally coordinated isolated Sn species,[55] thereby the framework Sn maintained their state through Cr loading. As shown in Figure 6b, the Cr-loaded samples showed peaks attributed to Si—O—Cr^{6+} vibration and Cr^{6+}—O or Cr^{6+} =O vibration at 949 cm^{-1} and 902 cm^{-1},[59] respectively, and their intensity increased with the increase in the Cr amount. To investigate the effects of Cr loading on the chemical state of Sn species, Sn 3d XPS spectra for Cr/Sn-Beta samples were recorded. The peaks derived from tetrahedrally coordinated framework Sn were shifted to lower binding energy by Cr loading, while extra-framework SnO_2 was detected at almost the same binding energy as before the Cr loading as shown in Figure 6c. In addition, Si 2p XPS peaks were also shifted to lower binding energy by Cr loading (Figure S2, Supporting Information). These low binding energies would be induced by the bonding of Sn—O—Cr and Si—O—Cr, suggesting the bonding of Cr to the defect sites in zeolites because Cr has a lower electronegativity than H. Because of the small amount of loaded Cr, Cr 2p XPS measurements reached their detecting limit (Figure S2, Supporting Information). The acidic properties of Cr/Sn-Beta samples were evaluated by FT-IR spectra of adsorbed pyridine (Figure 6d). All samples showed peaks of pyridine adsorbed on Lewis acid sites at ≈1450 cm^{-1},[56] while they have no Brønsted acidity. The loaded Cr had little impact on the Lewis acid amount of Cr/Sn-Beta(1), while Cr/Sn-Beta(1.5) showed smaller peaks compared to other samples because Lewis acidic open Sn—OH transformed to Sn—O—Cr. Therefore, although some loaded Cr formed Sn—O—Cr species from open-Sn sites, their amounts were not enough to have significant effects on the total Lewis acidity of zeolites, indicating that Cr—O—Si formed preferentially compared to the Cr—O—Sn. Josephson et al. investigated the open-site geometries in Sn-Beta zeolites using DFT calculations.[60] They revealed that isolated Sn—OH (behind Si—OH) is the most stable among all open Sn—OH sites. According to this research, Sn—OH in our synthesized Sn-Beta zeolites should exist in isolation. Cr^{6+} species are stabilized by multiple T-OH sites,[61] thereby the isolated Sn—OH species should not contribute to the stabilization of Cr^{6+} and maintain their activity as open Lewis acidic sites.

The effects of Cr loading amount on LDPE cracking activities of Sn-Beta-0.25F were evaluated using TG analysis (**Figure 7a**). The cracking temperatures were almost the same for Cr loadings lower than 1.0 wt.%, whereas 1.5 wt.% loadings reduced the activity of Sn-Beta-0.25F due to the reduction of Lewis acidity, therefore the excess amount of Cr loadings led to the deactivation. The changes in the color of the samples after LDPE cracking are shown in Figure 7c, indicating that coking was inhibited by Cr loadings. After the cracking reaction tests, the amount of deposited coke was measured using TG analysis and calculated the percentage of the mass of zeolites (Figure 7b). The coke amount decreased from 3.7% to under 2% with increasing Cr loading. Moreover, the UV–vis spectra of these spent catalysts revealed almost no change in the states of loaded Cr species compared to pre-used catalysts, indicating that Cr^{6+} connected to silanols maintained their structure through the LDPE cracking reaction (Figure 3).

© 2024 The Author(s). Advanced Sustainable Systems published by Wiley-VCH GmbH

23667486, 0, Downloaded from https://onlinelibrary.wiley.com/doi/10.1002/adsu.202400625 by The University Of Osaka, Wiley Online Library on [20/11/2024]. See the Terms and Conditions (https://onlinelibrary.wiley.com/terms-and-conditions) on Wiley Online Library for rules of use; OA articles are governed by the applicable Creative Commons License

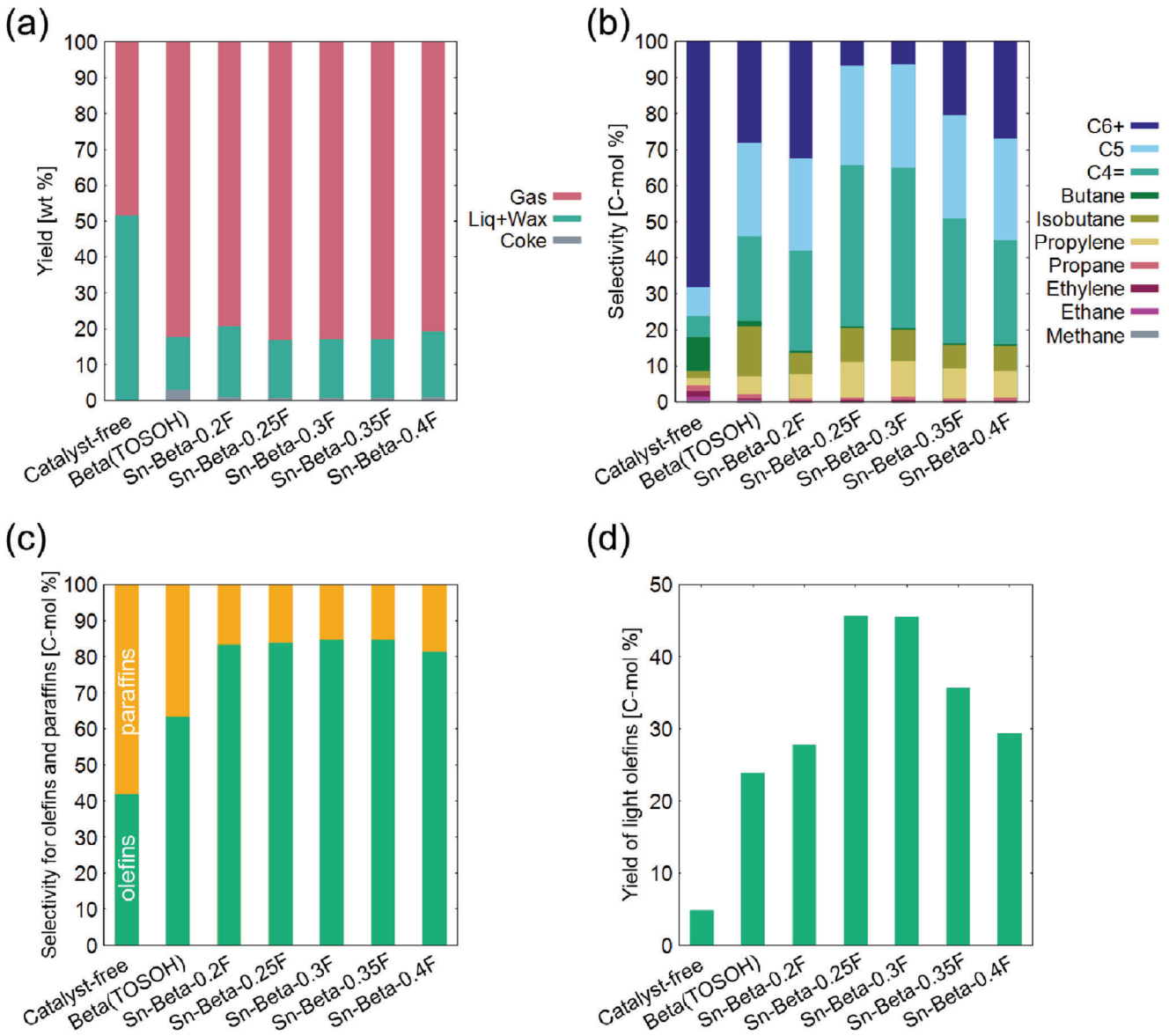

Figure 4. Product distributions over LDPE cracking with commercial Beta and Sn-Beta-*x*F. a) yields by group, b) gaseous product distribution, c) selectivity for olefins and paraffins (C2–C4), and d) yields of light olefins (C2–C4).

To investigate the activity of spent catalysts, LDPE cracking tests were repeated 3 times using Sn-Beta-0.25F (without Cr) and Cr/Sn-Beta(1) without oxidative regeneration of the catalysts (**Figure 8**). Sn-Beta-0.25F was significantly deactivated by coke deposition and showed almost no activity in the third reaction tests, whereas Cr/Sn-Beta(1) kept its activity through repetitive cracking. Moreover, the amount of deposited coke on Cr/Sn-Beta(1) remained at ≈3.2%, while that on Sn-Beta-0.25F significantly increased to nearly 10% as shown in Figure 8c.

The product distributions over repetitive LDPE cracking with Sn-Beta-0.25F and Cr/Beta(1) were analyzed using gas chromatography (**Figure 9**). The detailed analysis method was described in the experimental section. The gaseous product yields were decreased and their distributions were shifted to larger molecules with the decrease in the cracking activity by coke deposition on Sn-Beta-0.25F, whereas Cr/Sn-Beta(1) showed almost the same product distributions through repetitive LDPE cracking tests (Figure 9a,b). In addition, Cr loading increased olefin selectivity in C2–C4 by ≈5% attributed to the dehydrogenation ability of loaded Cr^{6+} species. Moreover, Cr/Sn-Beta(1) recorded over 45% light olefin yields on all three times LDPE cracking tests, while those with Sn-Beta-0.25F without Cr loading significantly decreased from 45% to 14.4% (Figure 9d).

3. Conclusion

In summary, Cr^{6+}- loaded Lewis acidic Sn-Beta zeolites were hardly deactivated and recorded over 45% light olefin yields on three times repetitive LDPE cracking tests without oxidative re-

© 2024 The Author(s). Advanced Sustainable Systems published by Wiley-VCH GmbH

23667486, 0, Downloaded from https://onlinelibrary.wiley.com/doi/10.1002/adsu.202400625 by The University Of Osaka, Wiley Online Library on [20/11/2024]. See the Terms and Conditions (https://onlinelibrary.wiley.com/terms-and-conditions) on Wiley Online Library for rules of use; OA articles are governed by the applicable Creative Commons License

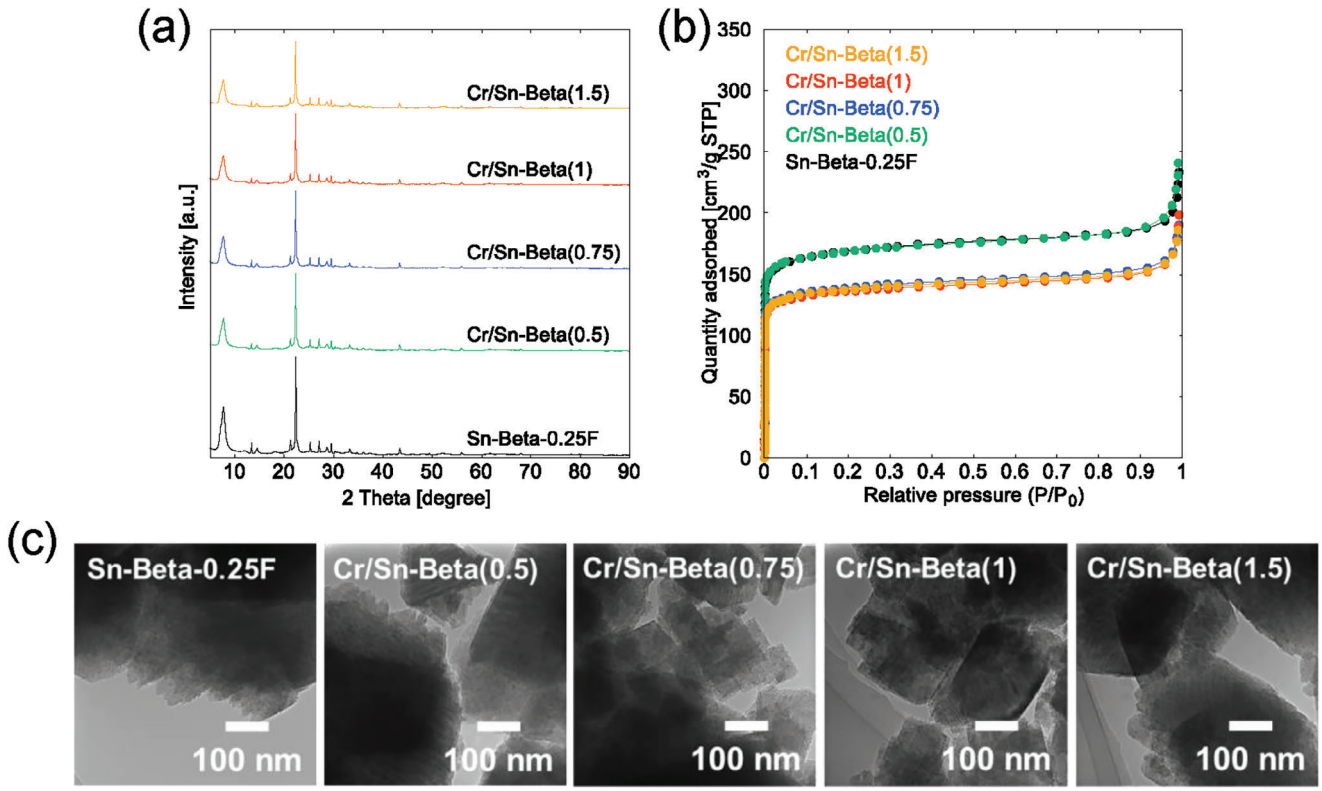

Figure 5. a). XRD patterns, b) N_2 adsorption isotherms, and c) TEM images of Sn-Beta-0.25F and Cr/Sn-Beta(*y*).

generation. By changing the crystallinity of Sn-Beta zeolites with different feed fluoride ions content in their synthesis, the active sites for LDPE cracking reaction were implicated as Lewis acidic open-Sn sites. These open-Sn sites in Sn-Beta zeolites catalyze the cracking reaction and produce light olefins selectively because the absence of Brønsted acid sites leads to the protection of olefins from ionization accompanied by conversion to other hydrocarbons. Moreover, although the excess Cr addition reduced the Lewis acidity of zeolites because open-Sn sites were converted to Sn—O—Cr, the appropriate amount of Cr^{6+} loading to Sn-Beta zeolites realized the coking inhibition while maintaining their catalytic activity on LDPE cracking. Therefore, the synergistic effect of Lewis acidic open-Sn sites and Cr^{6+} connected to zeolitic silanol groups led to selective and repetitive production of light olefins without oxidative regeneration. This study provides the catalyst design guidelines for the catalytic cracking of waste polyolefins.

4. Experimental Section

Materials: The following materials were used as received: H^+-type Beta zeolite (SiO_2/Al_2O_3 = 28.9, TOSOH corporation), nitric acid solution (35 wt%, FUJIFILM Wako Pure Chemical Corporation), boric acid (FUJIFILM Wako Pure Chemical Corporation), piperidine (Tokyo Chemical Industry Co., Ltd.), fumed silica (Sigma–Aldrich), hexamethyleneimine (HMI) (Sigma–Aldrich), tin(IV) chloride pentahydrate (FUJIFILM Wako Pure Chemical Corporation), tetraethylammonium hydroxide (TEAOH) solution (35 wt.%, Sigma–Aldrich), ammonium fluoride (FUJIFILM Wako Pure Chemical Corporation), chromium (III) acetate (FUJIFILM Wako Pure Chemical Corporation), low-density polyethylene (LDPE) powder (500 microns, d = 0.92 g cm^{-3}, Alfa Aesar).

Catalyst Preparation—Sn-Beta Zeolites: According to previous research,[62] Sn-Beta zeolites were synthesized via interzeolite transformation from Sn-MWW zeolites. Before Sn-MWW synthesis, B-MWW was synthesized and deboronated by acid treatment. An aqueous solution of 8.04 g of boric acid with 68.4 g of H_2O was stirred at room temperature (RT) for 30 min and then, 23.85 g of piperidine and 12 g of fumed silica were added. After further stirring at RT for 15 h, the mixture was placed in a Teflon-lined autoclave and crystalized at 170 °C for 7 days under rotation (10 rpm). The solid product was washed with deionized (DI) water three times using centrifugation and then, calcined at 600 °C for 5 h. The as-synthesized B-MWW was deboronated with 35 wt % HNO_3 solution (3 g B-MWW/ 100 g solution) at 180 °C for 24 h. After washing and drying, de-B-MWW was obtained. The de-B-MWW was added to the aqueous solution of $SnCl_4{\cdot}5H_2O$ (0.1551 g) and HMI (2.174 g) with 15.6 g of DI water. After stirring at RT for 30 min, the mixture was placed in a Teflon-lined autoclave and kept at 175 °C for 3 days under rotation (60 rpm). The product was washed with DI water and then, calcined at 550 °C for 8 h to obtain Sn-MWW.

Sn-Beta zeolites were synthesized by interzeolite transformation of as-synthesized Sn-MWW using siliceous deAl-Beta seeds. Here, deAl-Beta seeds were prepared by treating the commercial Beta zeolite (TOSOH, SiO_2/Al_2O_3 = 28.9) with 35 wt % HNO_3 solution at 180 °C for 24 h. Sn-MWW was added to the mixture including 35 wt % TEAOH solution and deAl-Beta seeds (10 wt % related to SiO_2 of MWW). After stirring the mixture at RT for 5 min, the appropriate amount of NH_4F was added. The molar ratio of the final solution was 1.0 SiO_2:0.3 TEAOH:*x* NH_4F (*x* = 0.2, 0.25, 0.3, 0.35, and 0.4). The mixtures were dried at 80 °C for 1 h after 30 min stirring. The dry gel was placed in a Teflon-lined autoclave and heated at 190 °C for 12 h. The products were washed with DI water and then, calcined at 550 °C for 8 h. The final products were named Sn-Beta-*x*F.

© 2024 The Author(s). Advanced Sustainable Systems published by Wiley-VCH GmbH

23667486, 0, Downloaded from https://onlinelibrary.wiley.com/doi/10.1002/adsu.202400625 by The University Of Osaka, Wiley Online Library on [20/11/2024]. See the Terms and Conditions (https://onlinelibrary.wiley.com/terms-and-conditions) on Wiley Online Library for rules of use; OA articles are governed by the applicable Creative Commons License

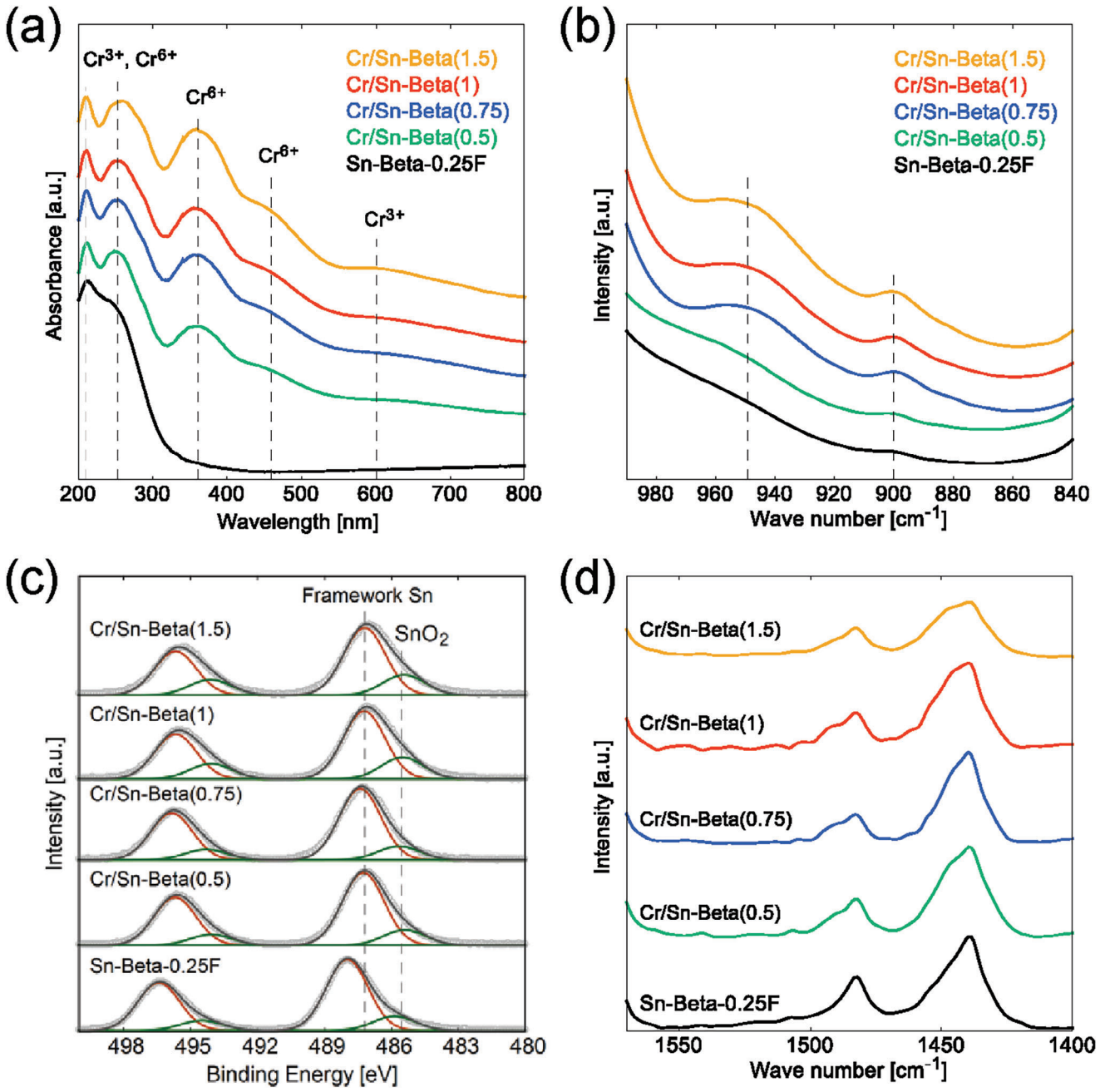

Figure 6. a). UV–vis, b) FT-IR, and c) Sn 3d XPS spectra of Sn-Beta-0.25F. d) FT-IR spectra of adsorbed pyridine on Sn-Beta-0.25F and Cr/Sn-Beta(*y*).

Cr/Sn-Beta Zeolites: According to the previous report,[44,45] Cr/Sn-Beta zeolites were prepared by the incipient wetness impregnation method. Sn-Beta-0.25F was added to aqueous solutions of chromium (III) acetate at a Cr/zeolite mass ratio of *y*/100 ($y = 0.5$, 0.75, 1, and 1.5). After drying at 90 °C for 1 h, the samples were calcined at 550 °C for 5 h. The synthesized catalysts were named Cr/Sn-Beta(*y*).

Characterization: The crystal structures of synthesized zeolites were detected by X-ray diffraction (XRD) patterns measured on a PANalytical X'Pert-MPD diffractometer using Cu-Kα radiation. The transmission electron microscope (TEM) images were recorded on a Hitachi H800 electron microscope at an acceleration voltage of 200 kV. The Sn and Cr content were determined by energy-dispersive X-ray spectroscopy (EDS) analysis using a JEOL JCM-7000 instrument. The physical properties of the catalysts were evaluated by N_2 adsorption measurements at −196 °C using a BELSORP-Max (MicrotracBel). The samples were heated to 250 °C for 3 h under vacuum before the N_2 adsorption measurements. The diffuse reflectance ultraviolet-visible (UV–vis) spectra of the zeolites were recorded using a JASCO V-770 spectrophotometer. Fourier-transform infrared (FT-IR) spectra of the pyridine adsorbed on zeolitic acid sites were measured using a mercury-cadmium-telluride (MCT) detector with an average of 128 scans at a resolution of 4 cm^{-1} in the wavenumber range 4000–400 cm^{-1}. Before FT-IR spectroscopy, pyridine adsorption onto the zeolites was conducted and then, purged with He at 100 °C for 15 min to remove excess pyridine.

© 2024 The Author(s). Advanced Sustainable Systems published by Wiley-VCH GmbH

23667486, 0, Downloaded from https://onlinelibrary.wiley.com/doi/10.1002/adsu.202400625 by The University Of Osaka, Wiley Online Library on [20/11/2024]. See the Terms and Conditions (https://onlinelibrary.wiley.com/terms-and-conditions) on Wiley Online Library for rules of use; OA articles are governed by the applicable Creative Commons License

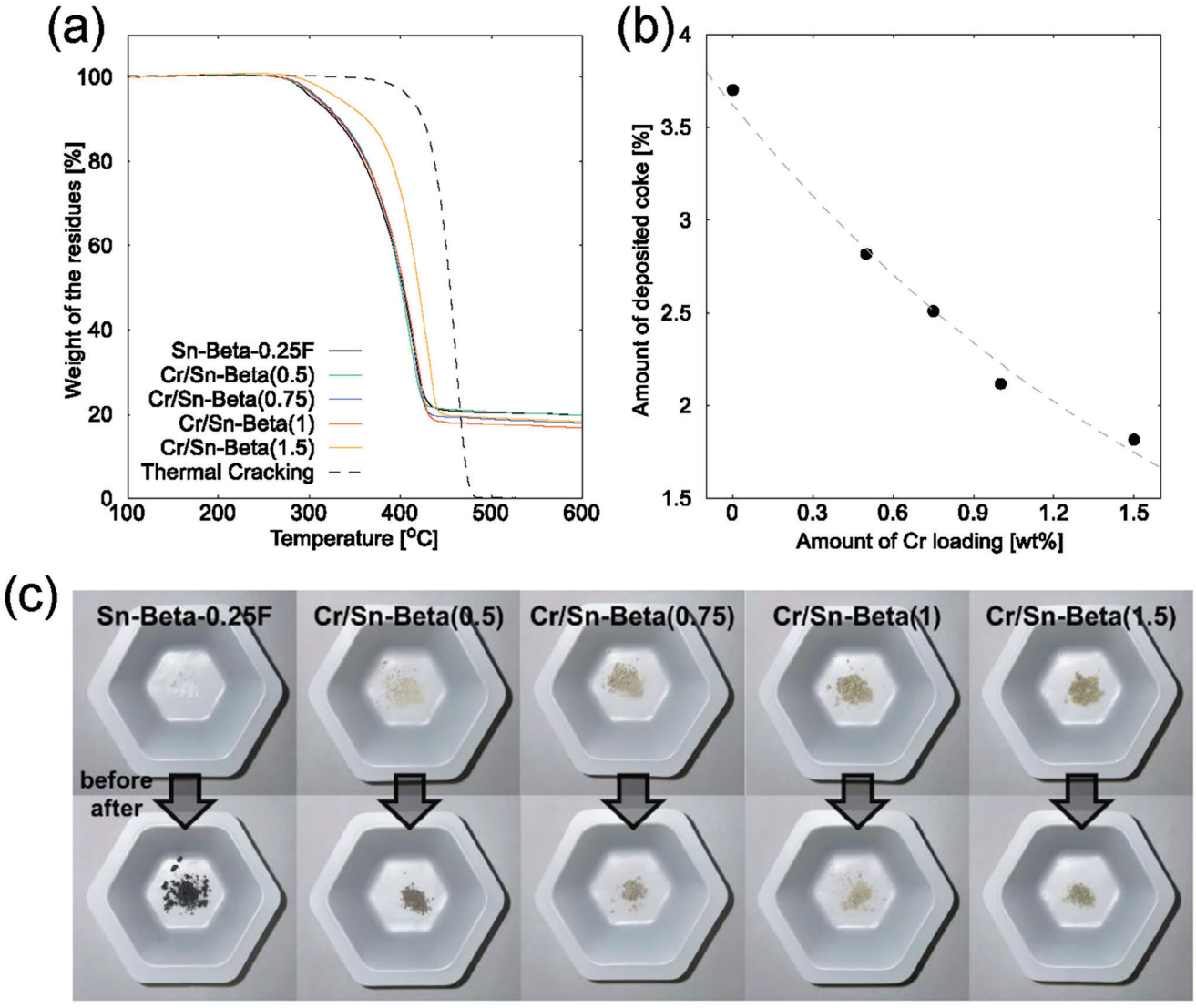

Figure 7. a). TG curves were obtained during the catalytic cracking of LDPE with Sn-Beta-0.25F and Cr/Sn-Beta(*y*). b) Relationship between Cr loading amount and deposited coke amount. c) Changes in the color of Sn-Beta-0.25F and Cr/Sn-Beta(*y*) before and after LDPE cracking.

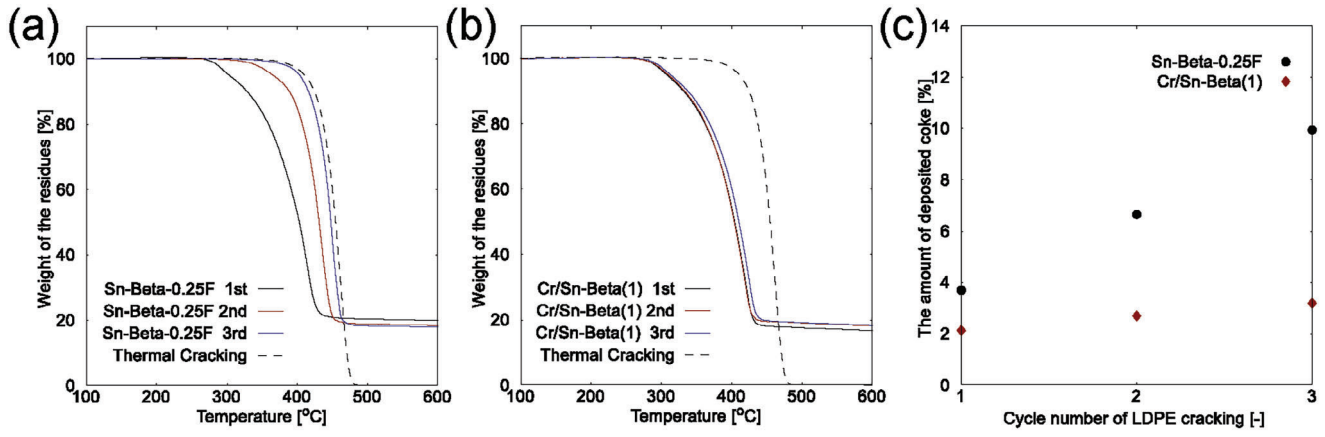

Figure 8. TG curves were obtained in the repetitive LDPE cracking with a) Sn-Beta-0.25F and b) Cr/Sn-Beta(1). c) Deposited coke amount during repetitive LDPE cracking on Sn-Beta-0.25F and Cr/Sn-Beta(1).

© 2024 The Author(s). Advanced Sustainable Systems published by Wiley-VCH GmbH

23667486, 0, Downloaded from https://onlinelibrary.wiley.com/doi/10.1002/adsu.202400625 by The University Of Osaka, Wiley Online Library on [20/11/2024]. See the Terms and Conditions (https://onlinelibrary.wiley.com/terms-and-conditions) on Wiley Online Library for rules of use; OA articles are governed by the applicable Creative Commons License

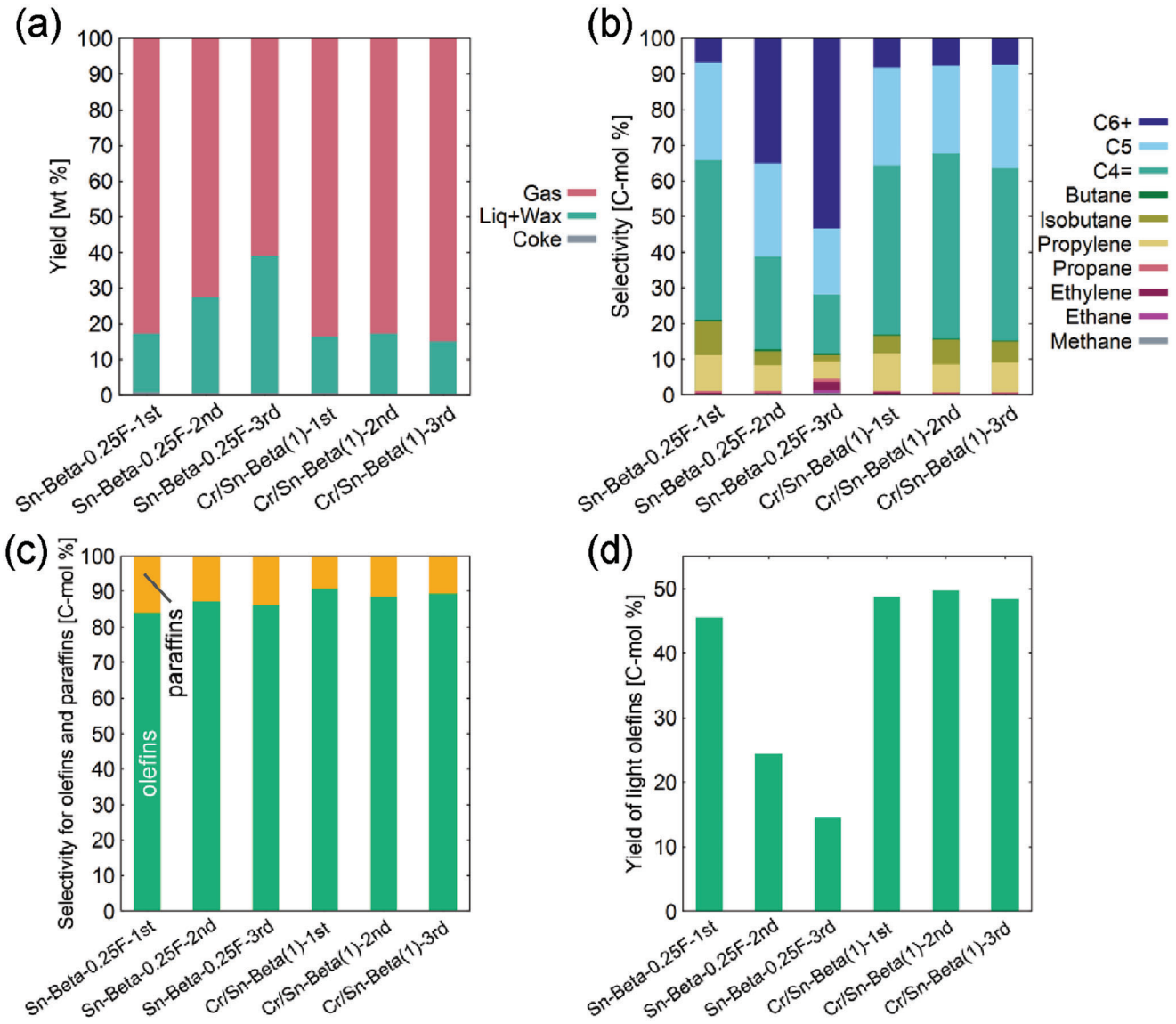

Figure 9. Product distributions over repetitive LDPE cracking tests with Sn-Beta-0.25F and Cr/Sn-Beta(γ). a) yields by group, b) gaseous product distribution, c) selectivity for olefins and paraffins (C2–C4), and d) yields of light olefins (C2–C4).

LDPE Catalytic Cracking—Evaluation of Cracking Temperatures (TG): The zeolites and LDPE powder were mixed at zeolite/LDPE = 1/4 (mass basis). The LDPE cracking activities of synthesized zeolites were evaluated by thermogravimetric (TG) analysis using a DTG-60A (SHIMADZU). The mixture was heated to 600 °C with 5 °C m^{-1}in under a N_2 flow (60 ml min^{-1}), and the cracking temperature was determined.

Analysis of Product Distributions (GC): The product distributions were analyzed using gas chromatography. The zeolite/LDPE mixture was placed in an alumina tube with an inner diameter of 24 mm and heated to 600 °C (5 °C min^{-1}) under N_2 flow (60 ml min^{-1}). During the cracking reaction, the exit gas was collected in a gas bag through a cold trap with ice water. The yields of solid and liquid products (Y_{S+L}) were calculated based on the mass increase of the trap after the reaction. The yields of coke deposited on zeolites (Y_C) were also calculated on a mass basis. The amount of coke deposited was evaluated using TG. The spent zeolites were heated to 600 °C with 5 °C min^{-1} under ambient atmosphere. The weight loss from 350 to 600 °C was attributed to the combustion of the deposited coke. The yields of gaseous products (Y_G) were calculated by the following equation: $Y_G = 100 - (Y_{S+L}+Y_C)$. The selectivity of each gas product (X) was detected using a Shimadzu GC-2025 gas chromatograph equipped with a flame ionization detector and calculated the yields of light olefins (Y_{LO}) by the following equation: $Y_{LO} = Y_G\ (X_{C_2H_4}+X_{C_3H_6}+X_{C_4H_8})$.

Supporting Information

Supporting Information is available from the Wiley Online Library or from the author.

Acknowledgements

A part of the present experiments was carried out by using a facility in the Research Center for Ultra-High Voltage Electron Microscopy, Osaka University.

© 2024 The Author(s). Advanced Sustainable Systems published by Wiley-VCH GmbH

23667486, 0, Downloaded from https://onlinelibrary.wiley.com/doi/10.1002/adsu.202400625 by The University Of Osaka, Wiley Online Library on [20/11/2024]. See the Terms and Conditions (https://onlinelibrary.wiley.com/terms-and-conditions) on Wiley Online Library for rules of use; OA articles are governed by the applicable Creative Commons License

Conflict of Interest

The authors declare no conflict of interest.

Data Availability Statement

The data that support the findings of this study are available from the corresponding author upon reasonable request.

Keywords

catalytic cracking, coking inhibition, lewis acid, light olefin, polyolefin, zeolites

Received: August 21, 2024
Revised: October 3, 2024
Published online:

[1] G. Lopez, M. Artetxe, M. Amutio, J. Bilbao, M. Olazar, *Renewable Sustainable Energy Rev.* **2017**, *73*, 346.
[2] D. P. Serrano, J. Aguado, J. M. Escola, *ACS Catal.* **2012**, *2*, 1924.
[3] G. Elordi, M. Olazar, P. Castaño, M. Artetxe, J. Bilbao, *Ind. Eng. Chem. Res.* **2012**, *51*, 14008.
[4] Y. Peng, Y. Wang, L. Ke, L. Dai, Q. Wu, K. Cobb, Y. Zeng, R. Zou, Y. Liu, R. Ruan, *Energy Convers. Manage.* **2022**, *254*, 115243.
[5] M. Chu, W. Tu, S. Yang, C. Zhang, Q. Li, Q. Zhang, J. Chen, *SusMat* **2022**, *2*, 161.
[6] A. Musa, E. A. Jaseer, S. Barman, N. Garcia, *Energy Fuels* **2024**, *38*, 1676.
[7] Z. Dong, W. Chen, K. Xu, Y. Liu, J. Wu, F. Zhang, *ACS Catal.* **2022**, *12*, 14882.
[8] G. Yang, P. Peng, H. Guo, H. Song, Z. Li, *Polym. Degrad. Stab.* **2024**, *222*, 110712.
[9] J. Aguado, D. P. Serrano, G. S. Miguel, J. M. Escola, J. M. Rodríguez, *J. Anal. Appl. Pyrolysis* **2007**, *78*, 153.
[10] Y. Wang, Y. Zhang, H. Fan, P. Wu, M. Liu, X. Li, J. Yang, C. Liu, P. Bai, Z. Yan, *Catal. Today* **2022**, *405–406*, 135.
[11] M. Boronat, A. Corma, *Appl. Catal., A* **2008**, *336*, 2.
[12] D. P. Serrano, J. Aguado, J. M. Escola, *Ind. Eng. Chem. Res.* **2000**, *39*, 1177.
[13] G. Manos, A. Garforth, J. Dwyer, *Ind. Eng. Chem. Res.* **2000**, *39*, 1198.
[14] M. M. Hasan, N. Batalha, G. Fraga, M. H. M. Ahmed, L. Pinard, M. Konarova, S. Pratt, B. Laycock, *Sustainable Energy Fuels* **2022**, *6*, 1587.
[15] Q. Snu, N. Wang, R. Bai, Y. Hui, T. Zhang, D. A. Do, P. Zhang, L. Song, S. Miao, J. Yu, *Adv. Sci.* **2019**, *6*, 1802350.
[16] X. Liu, Z. Zhu, *Adv. Sci.* **2024**, *11*, 2306533.
[17] S. Kokuryo, H. A. Jabri, K. Miyake, Y. Uchida, S. Tanaka, M. Miyamoto, Y. Oumi, N. Nishiyama, *ChemistrySelect* **2022**, *7*, 202200756.
[18] P. Gao, Q. Wang, J. Xu, G. Qi, C. Wang, X. Zhou, X. Zhao, N. Feng, X. Liu, F. Deng, *ACS Catal.* **2017**, *8*, 69.
[19] A. Veses, B. Puértolas, J. M. López, M. S. Callén, B. Solsona, T. García, *ACS Sustainable Chem. Eng.* **2016**, *4*, 1653.
[20] B. Tang, W. Dai, X. Sun, N. Guan, L. Li, M. Hunger, *Green Chem.* **2014**, *16*, 2281.
[21] L. Meng, X. Zhu, E. J. M. Hensen, *ACS Catal.* **2017**, *7*, 2709.
[22] M. S. Abbas-Abadi, Y. Ureel, A. Eschenbacher, F. H. Vermeire, R. J. Varghese, J. Oenema, G. D. Stefanidis, K. M. Van Geem, *Prog. Energy Combust. Sci.* **2023**, *96*, 101046.
[23] M. Fakhroleslam, S. M. Sadrameli, *Ind. Eng. Chem. Res.* **2020**, *59*, 12288.
[24] K. P. de Jong, *Science* **2016**, *351*, 1030.
[25] C. P. Nicholas, *Appl. Catal., A* **2017**, *543*, 82.
[26] K. H. Song, S. K. Jeong, B. H. Jeong, K.-Y. Lee, H. J. Kim, *Catalysts* **2020**, *10*, 1149.
[27] A. Corma, A. V. Orchillés, *Microporous Mesoporous Mater.* **2000**, *35*, 21.
[28] F. C. Jentoft, B. C. Gates, *Top. Catal.* **1997**, *4*, 1.
[29] M. Marczewski, *J. Chem. Soc., Faraday Trans.* **1986**, *82*, 1687.
[30] S. Kokuryo, K. Tamura, S. Tsubota, K. Miyake, Y. Uchida, A. Mizusawa, T. Kubo, N. Nishiyama, *Catal. Sci. Technol.* **2024**, *14*, 3589.
[31] F. Berger, J. Sauer, *Angew. Chem.* **2021**, *133*, 3571.
[32] S. Vernuccio, E. E. Bickel, R. Gounder, L. J. Broadbelt, *ACS Catal.* **2019**, *9*, 8996.
[33] C. Chizallet, C. Bouchy, K. Larmier, G. Pirngruber, *Chem. Rev.* **2023**, *123*, 6107.
[34] S. Kokuryo, K. Miyake, Y. Uchida, A. Mizusawa, T. Kubo, N. Nishiyama, *Mater. Today Sustain.* **2022**, *17*, 100098.
[35] S. Kokuryo, K. Miyake, Y. Uchida, S. Tanaka, M. Miyamoto, Y. Oumi, A. Mizusawa, T. Kubo, N. Nishiyama, *ACS Omega* **2022**, *7*, 12971.
[36] S. Kokuryo, K. Tamura, K. Miyake, Y. Uchida, A. Mizusawa, T. Kubo, N. Nishiyama, *New J. Chem.* **2022**, *46*, 3838.
[37] S. Kokuryo, K. Tamura, K. Miyake, Y. Uchida, A. Mizusawa, T. Kubo, N. Nishiyama, *Catal. Sci. Technol.* **2022**, *12*, 4138.
[38] V. Daligaux, R. Richard, M.-H. Manero, *Catalysts* **2021**, *11*, 770.
[39] D. P. Serrano, J. Aguado, J. M. Rodríguez, A. Peral, *J. Anal. Appl. Pyrolysis* **2007**, *79*, 456.
[40] G. Elordi, M. Olazar, G. Lopez, P. Castaño, J. Bilbao, *Appl. Catal., B* **2011**, *102*, 224.
[41] Y. Uemichi, M. Hattori, T. Itoh, J. Nakamura, M. Sugioka, *Ind. Eng. Chem. Res.* **1998**, *37*, 867.
[42] M. Guisnet, L. Costa, F. R. Ribeiro, *J. Mol. Catal. A: Chem.* **2009**, *305*, 69.
[43] B. Liu, D. Slocombe, M. AlKinany, H. AlMegren, J. Wang, J. Arden, A. Vai, S. Gonzalez-Cortes, T. Xiao, V. Kuznetsov, P. P. Edwards, *Appl. Petrochem. Res.* **2016**, *6*, 209.
[44] S. Kokuryo, K. Tamura, K. Miyake, Y. Uchida, M. Miyamoto, Y. Oumi, A. Mizusawa, T. Kubo, N. Nishiyama, *Catal. Sci. Technol.* **2022**, *12*, 7270.
[45] S. Kokuryo, K. Tamura, S. Tsubota, K. Miyake, Y. Uchida, A. Mizusawa, T. Kubo, N. Nishiyama, *ChemCatChem* **2023**, *15*, 202300461.
[46] Y. Cheng, C. Miao, W. Hua, Y. Yue, Z. Gao, *Appl. Catal., A* **2017**, *532*, 111.
[47] B. M. Weckhuysen, I. E. Wachs, R. A. Schoonheydt, *Chem. Rev.* **1996**, *96*, 3327.
[48] X. Sun, J. Xue, Y. Ren, X. Li, L. Zhou, B. Li, Z. Zhao, *Mol. Catal.* **2021**, *505*, 111520.
[49] J. M. Newsman, M. M. J. Treacy, W. T. Koetsier, C. B. D. Gruyter, *Proc. R. Soc. Lond. A.* **1988**, *420*, 375.
[50] J. B. Higgins, R. B. LaPierre, J. L. Schlenker, A. C. Rohrman, J. D. Wood, G. T. Kerr, W. J. Rohrbaugh, *Zeolites* **1988**, *8*, 446.
[51] B. Louis, L. Kiwi-Minsker, *Microporous Mesoporous Mater.* **2004**, *74*, 171.
[52] T. Blasco, M. A. Camblor, A. Corma, P. Esteve, A. Martínez, C. Prieto, S. Valencia, *Chem. Commun.* **1996**, *20*, 2367.
[53] S. Prodinger, H. Shi, H. Wang, M. A. Derewinski, J. A. Lercher, *Appl. Catal., B* **2018**, *237*, 996.
[54] Z. Kang, X. Zhang, H. Liu, J. Qiu, K. L. Yeung, *Chem. Eng. J.* **2013**, *218*, 425.
[55] B. Tang, S. Li, W.-C. Song, E.-C. Yang, X.-J. Zhao, N. Guan, L. Li, *ACS Sustainable Chem. Eng.* **2020**, *8*, 3796.
[56] B. Tang, W. Dai, G. Wu, N. Guan, L. Li, M. Hunger, *ACS Catal.* **2014**, *4*, 2801.

© 2024 The Author(s). Advanced Sustainable Systems published by Wiley-VCH GmbH

23667486, 0, Downloaded from https://onlinelibrary.wiley.com/doi/10.1002/adsu.202400625 by The University Of Osaka, Wiley Online Library on [20/11/2024]. See the Terms and Conditions (https://onlinelibrary.wiley.com/terms-and-conditions) on Wiley Online Library for rules of use; OA articles are governed by the applicable Creative Commons License

[57] T. A. Nijhuis, S. J. Tinnemans, T. Visser, B. M. Weckhuysen, *Chem. Eng. Sci.* **2004**, *59*, 5487.
[58] B. M. Weckhuysen, A. Bensalem, R. A. Schoonheydt, *J. Chem. Soc., Faraday Trans.* **1998**, *94*, 2011.
[59] Z. Deng, X. Ge, W. Zhang, S. Luo, J. Shen, F. Jing, W. Chu, *Chin. J. Chem. Eng.* **2021**, *34*, 77.
[60] T. R. Josephson, G. R. Jenness, D. G. Vlachos, S. Caratzoulas, *Microporous Mesoporous Mater.* **2017**, *245*, 45.
[61] S. De, S. Ould-Chikh, A. Aguilar, J. L. Hazemann, A. Zitolo, A. Ramirez, S. Telavoic, J. Gascon, *ACS Catal.* **2021**, *11*, 3988.
[62] Y. Cho, S. Kweon, J. S. Park, M. B. Park, *ACS Sustainable Chem. Eng.* **2023**, *11*, 17797.

© 2024 The Author(s). Advanced Sustainable Systems published by Wiley-VCH GmbH

23667486, 0, Downloaded from https://onlinelibrary.wiley.com/doi/10.1002/adsu.202400625 by The University Of Osaka, Wiley Online Library on [20/11/2024]. See the Terms and Conditions (https://onlinelibrary.wiley.com/terms-and-conditions) on Wiley Online Library for rules of use; OA articles are governed by the applicable Creative Commons License